

Study of Active Suspension Control Methods to Suppress Superconducting Maglev Vehicle Vibrations

No. 31

Erimitsu Suzuki, Ken Watanabe, and Hironori Hoshino

Railway Technical Research Institute, Maglev Systems Technology Division, Electromagnetic Applications Laboratory, 2-8-38 Hikari-cho, Kokubunji-shi, Tokyo, 185-8540, Japan esuzuki@rtri.or.jp

Masao Nagai

Tokyo University of Agriculture and Technology, Department of Mechanical Systems Engineering, 2-24-16 Naka-cho, Koganei-shi, Tokyo, 184-8588, Japan

ABSTRACT: In the continuing efforts toward the commercial operation of the superconducting Maglev system, in which vehicles travel at high speeds of over 500 km/h, methods of suppressing vehicle vibrations are being examined with respect to suitability for a public mode of transportation. Results are presented on methods for suppressing vehicle vibrations of the Maglev train, examining techniques such as vibration control of the primary suspension using electromagnetic forces output by a bogie-integrated linear generator, and preview control of the secondary suspension by actuators using data transmitted from the front to the rear of the train.

1 INTRODUCTION

In initial vehicle running tests, vibrations of the superconducting Maglev vehicle were controlled mainly focusing on the secondary suspension, and the control methods have been effective only for vibrations of relatively low frequencies at around 1 to 2 Hz corresponding to the natural car body vibration mode. The lightweight structure of the car bodies result in vibrations at around 4 to 5 Hz corresponding to the natural bogie vibration mode, and at other relatively higher frequencies that influence the ride comfort.

A device called a linear generator that was developed and integrated into an existing bogie of the Maglev system generates on-board power and can also produce additional electromagnetic forces that can be used in the control of the primary suspension. This device has previously been demonstrated in full-scale vehicle experiments to effectively apply electromagnetic damping directly to the primary suspension, and reduce vibrations of relatively higher frequencies that are otherwise difficult to reduce by controlling only the secondary suspension. Studies on this primary suspension control device in conjunction

with secondary suspension control and the effects on reducing vehicle vibrations are discussed in this report.

The Maglev train set has an articulated bogie arrangement to provide a low center of gravity and improved magnetic shielding performance. The bogies are evenly spaced along the train set. In addition, because of the interactions of electromagnetic forces in the primary suspension, each bogie of the Maglev train set is subjected to nearly the same external disturbance, with practically equal time differences between consecutive bogies. Utilizing these properties, techniques for preview control of the secondary suspension are examined that measure external disturbances at the front of the Maglev train set and feed the data to the rear of the train, to enhance the vehicle ability to efficiently minimize the impact of deviations in the guideway ground coil alignment.

Results are presented on the methods for reducing vehicle vibrations of the superconducting Maglev train, examining the vibration control of the primary suspension using electromagnetic forces output by a bogie-integrated linear generator, combined with the preview control of the secondary suspension. Effective implementation of these vibration reduction methods on Maglev vehicles are expected to improve

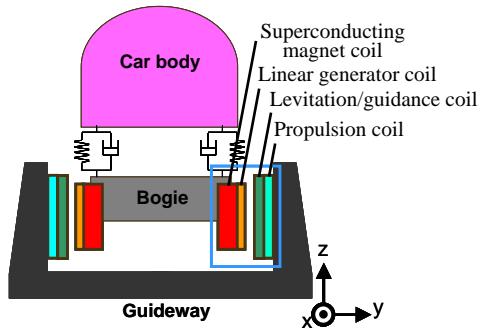


Figure 1. View of the superconducting Maglev system.

ride comfort, and eventually lead to the reduction of construction costs by enabling the relaxation of the limits of tolerated irregularities in the guideway alignment, and the reduction of management costs by minimizing guideway maintenance. Such cost reductions are expected to outweigh the increase in vehicle costs due to installation of vibration control systems.

2 MECHANISM OF THE BOGIE-INTEGRATED LINEAR GENERATOR DEVICE IN THE CONTROL OF THE PRIMARY SUSPENSION

As shown in the cross-sectional view of the superconducting Maglev system in Figure 1, levitation/guidance coils and propulsion coils are installed on the sidewalls of a concrete guideway. The vehicle is equipped with superconducting magnet (SCM) coils and linear generator coils attached to the outer vessel surface of the SCM as part of the Maglev bogie-integrated linear generator device that generates power in the traveling vehicle using the harmonic magnetic fields in the levitation/guidance coils. This device can also be used to generate additional electromagnetic forces in the primary suspension to be used as control forces in reducing vehicle vibrations. The principles of additional electromagnetic forces output by the linear generator are shown in Figure 2 (Suzuki [4]). The

equivalent configuration of the linear generator coil for the function of generating additional forces is expressed in Figure 2a. Electrical current of amplitudes much smaller than that in the SCM coil is run through the linear generator coils. The resulting change in magnetic flux causes the already existing current in the levitation/guidance coil to increase slightly, indicated by the wide circular arrows in Figs. 2a and 2b. These additional currents generate additional forces indicated by the smaller additional arrows in Figure 2c, resulting in an additional upward force acting on the bogie. Likewise, additional downward force acting on the bogie can be generated by reversing the direction of the current flowing in the linear generator coil. By varying the amplitude and direction of the current in the linear generator coils according to the vertical motion of the vehicle bogie, this device can be used to control vertical vehicle vibrations.

This method has the advantage of requiring no additional systems solely for the purpose of generating electromagnetic forces. Furthermore, because the magnetic force is generated electrically, this method has minimal delay in response for high frequency ranges of vibration, in comparison to conventional methods using hydraulic or pneumatic systems (Suzuki [5]). Full-scale vehicle running tests on the Yamanashi Maglev Test Line confirmed the principles of magnetic forces output by the bogie-integrated linear generator device in the Japanese fiscal year 2001 (Hasegawa [1]). Vehicle running tests then confirmed the ability of the linear generator device to control vibrations using the generated forces in the fiscal year 2004 (Sakamoto [2]).

3 ANALYSES OF VEHICLE DYNAMICS

3.1 Vehicle model used in the computations

A vehicle model of a three-car train set for vertical and pitching motions with a total of 14 degrees of

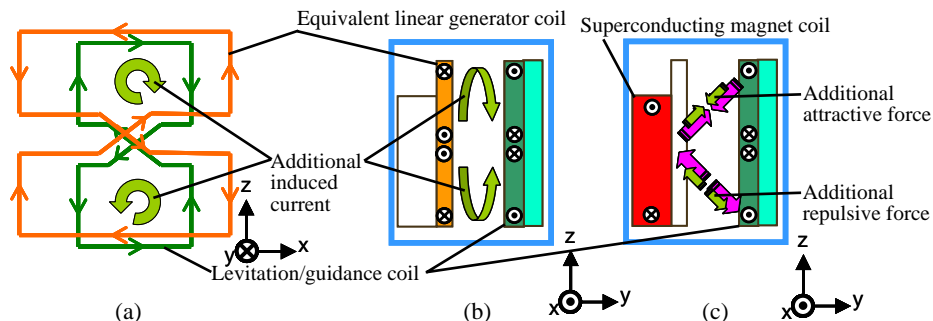


Figure 2. Mechanism of additional upward force acting on the bogie, generated by linear generator coils and used for vibration control.

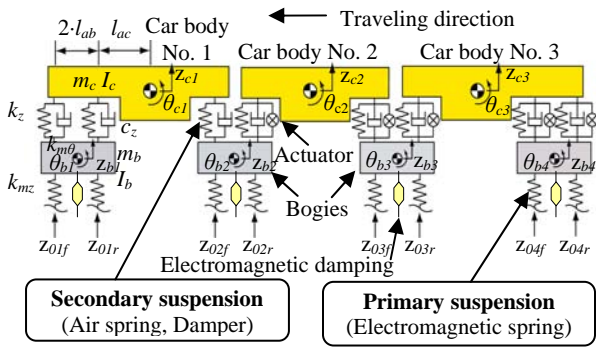


Figure 3. Vehicle model used in the computations.

freedom was used, as shown in Figure 3. The primary suspension between the bogie and guideway surface consists of electromagnetic spring characteristics resulting from interactions between the superconducting magnets and ground coils. The spring characteristics of the vertical and pitching motions are coupled with each other. The magnetic spring acts in equal distribution along the length of the bogie from front to rear. However, for purposes of optimizing computations, equivalent spring characteristics were approximated by concentrating the springs at two positions, one on the front and the other on the rear of the bogie. The secondary suspension between the car body and bogie consists of air springs that were approximated using a damper and a spring connected in parallel. Actuators for vibration control were added to the secondary suspension of the middle and rear cars (No. 2 and 3) and were assumed to have ideal operating properties with no time delay. In the primary suspension control model, the forces output by the bogie-integrated linear generator were used in all four bogies as damping forces in the vibration control.

The aforementioned magnetic forces output by the linear generator were assumed to be ideal, and delays in response were not considered. Furthermore, these magnetic forces of the linear generator are assumed to be equally distributed along the length of the bogie surface, such that the force at any longitudinal position on the bogie surface is of the same magnitude and same direction at any given time. For example, if an upward control force acts on the front end of a bogie at a given instance in time, an upward force of equal magnitude simultaneously acts on the rear end. Therefore, this force is assumed to have no influence on the bogie pitching motion. In the computation model, an equivalent vertical control force was concentrated on one point at the center of

mass of each of the four bogies. Although the force only controls the vertical motion, the pitching vibrations are expected to be much smaller than the vertical vibrations in the passive case, making vertical control a priority. The vehicle traveling speed was set to a constant 500 km/h.

3.2 Vehicle model parameters

The vehicle model parameters used in the computations are shown in Table 1. The values are based on those used by Watanabe [7].

Table 1: Vehicle model parameters

Parameter	Value
m_c [kg]	14.0×10^3
m_b [kg]	6.0×10^3
I_c [$\text{kg} \cdot \text{m}^2$]	82.0×10^4
I_b [$\text{kg} \cdot \text{m}^2$]	13.2×10^3
k_z [N/m]	0.4×10^6
k_{mz} [N/m]	4.7×10^6
$k_{m\theta}$ [N·m/rad]	1.0×10^7
c_z [N·s/m]	1.0×10^4
l_{ac} [m]	8.8
l_{ab} [m]	2.03

4 CONTROL SYSTEM

4.1 Frequency-shaped optimal preview control of the secondary suspension

When the objective is to improve vehicle ride comfort, optimal control laws usually include an evaluation function based on the car body acceleration. Because human perception of vibrations differs according to the frequency, vibrations can be efficiently reduced by evaluating acceleration data modified by frequency shaping techniques, resulting in a control method that takes ride comfort factors into consideration. In this study, a frequency shaping function $\bar{Q}(s)$ was derived as shown in Equation 1, with gain characteristics based on ride comfort level curve shown in Figure 4, used by the former Japanese National Railways to define frequency-dependant human sensitivity to vibrations.

$$\bar{Q}(s) = \frac{s + w_{n1}}{w_{n1}} \cdot \frac{K_1 w_{n2}^2}{s^2 + 2\zeta_1 w_{n2} s + w_{n2}^2} \quad (1)$$

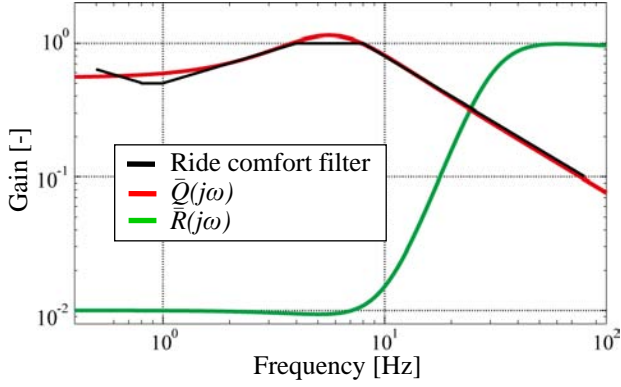


Figure 4. Ride comfort filter and frequency shaping functions $\bar{Q}(j\omega)$, $\bar{R}(j\omega)$

Here, $K_1 = 0.55$, $w_{n1} = 5.2\pi$, $w_{n2} = 12\pi$, and $\zeta_1 = 0.61$. In order to suppress the actuator output at high frequencies, a frequency shaping function $\bar{R}(s)$ was also applied to the control input.

$$\bar{R}(s) = \frac{K_2 w_{n3}^4 (s^2 + 2\zeta_3 w_{n4} s + w_{n4}^2)^2}{w_{n4}^4 (s^2 + 2\zeta_2 w_{n3} s + w_{n3}^2)^2} \quad (2)$$

Here, $K_2 = 0.01$, $w_{n3} = 62\pi$, $w_{n4} = 20\pi$, and $\zeta_2 = \zeta_3 = 0.6$. The shaping factor gain increases from around 10 Hz to 30 Hz, where the ride comfort level curve drops, and levels off at around 30 Hz, in effect a high pass filter. Next, inverse Laplace transforms of Equations 1 and 2 were derived to express the equations in state-space form. The state equation for $\bar{Q}(s)$ can be expressed using the input Y , state X_q , and coefficient matrices A_q , B_q , C_q , and D_q :

$$\begin{aligned} \dot{X}_q &= A_q X_q + B_q Y \\ Y_q &= C_q X_q + D_q Y \end{aligned} \quad (3)$$

In the same manner, the state equation for $\bar{R}(s)$ can be expressed as:

$$\begin{aligned} \dot{X}_r &= A_r X_r + B_r u \\ Y_r &= C_r X_r + D_r u \end{aligned} \quad (4)$$

The state equations for the vehicle model shown in Figure 3 can be expressed as:

$$\begin{aligned} \dot{X} &= AX + Bu + W\dot{x}_0 \\ Y &= CX + Du + Z\dot{x}_0 \end{aligned} \quad (5)$$

Here, X represents the state variables, Y the output used in Equation 3, u the control input, the rate of change of the external disturbance x_0 with respect to time, and A , B , C , D , and Z the coefficient matrices. By substituting Y in Equation 3 with the output of Equation 5, frequency shaping factors are applied to

the output. Combining Equations 3, 4, and 5 results in the form:

$$\begin{Bmatrix} \dot{X} \\ \dot{X}_q \\ \dot{X}_r \end{Bmatrix} = \begin{bmatrix} A & 0 & 0 \\ B_q C & A_q & 0 \\ 0 & 0 & A_r \end{bmatrix} \begin{Bmatrix} X \\ X_q \\ X_r \end{Bmatrix} + \begin{bmatrix} B \\ B_q D \\ B_r \end{bmatrix} u + \begin{bmatrix} W \\ B_q Z \\ 0 \end{bmatrix} \dot{x}_0 \quad (6)$$

This state equation is discretized to construct an optimal preview control system (Shirasaki [3]). Finally, an evaluation function J is used to derive feedback and feed-forward coefficients. This function evaluates values resulting from frequency shaping factors added to the output Y and the input u , and is expressed as:

$$\begin{aligned} J &= \sum_{k=-M_R+1}^{\infty} \left\{ q \left[\sum_{n=0}^{k-1} \bar{Q}(n) Y(k-n) \right]^2 + r \left[\sum_{n=0}^{k-1} \bar{R}(n) u(k-n) \right]^2 \right\} \\ &= \sum_{k=-M_R+1}^{\infty} [q Y_q^2(k) + r Y_r^2(k)] \end{aligned} \quad (7)$$

Here, q and r are coefficient weighting matrices, and M_R is the number of preview steps. The optimal control input can be derived by solving the Riccati equation resulting from substituting the outputs of Equations 3 and 4 into Equation 7. Considering real-time performance and redundancy in this study, the frequency-shaped optimal preview control system was implemented using decentralized controllers. The vehicle model for computations is divided up as shown in Figure 5, such that a reduced-order sub-model unit exists now for each actuator, with two vertical degrees of freedom in each sub-model unit consisting of one car body component and one bogie component. A controller is designed independently for each sub-model unit. For example, the state variables of Controller No. 1 in Figure 5 are the vertical velocities and relative displacements of the car body and bogie:

$$x_{controller1} = [(\dot{z}_{c2}) (\dot{z}_{b2}) (z_{c2} - z_{b2}) (z_{b2} - z_{02r})]^T \quad (8)$$

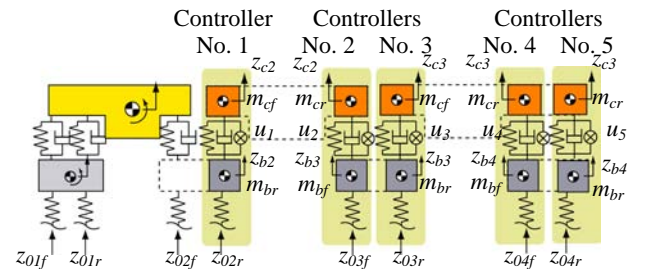


Figure 5. Model of decentralized controllers.

Decentralizing the control system results in four state variables as shown in Equation 8, and greatly simplifies the computations in comparison to designing the controller using the full order of the entire model. For this decentralized controller model, the control system is designed by the methods described earlier in this section. Here, the evaluation function of this control model is based on Equation 7 and expressed as follows:

$$J = \sum_{k=-M_R+1}^{\infty} \left\{ q_1 \left[\left(\sum_{n=0}^{k-1} \bar{Q}(n) \ddot{z}_{c2}(k-n) \right)^2 + \left(\sum_{n=0}^{k-1} \bar{Q}(n) \ddot{z}_{c3}(k-n) \right)^2 \right] + q_2 \left[(z_{c2}(k) - z_{b2}(k))^2 + (z_{c2}(k) - z_{b3}(k))^2 + (z_{c3}(k) - z_{b3}(k))^2 + (z_{c3}(k) - z_{b4}(k))^2 \right] + r \sum_{i=1}^5 \left(\sum_{n=0}^{k-1} \bar{R}(n) u_i(k-n) \right)^2 \right\} \quad (9)$$

Equation 9 includes frequency shaping of vertical accelerations of cars No. 2 and 3 and control inputs, and coefficient weighting of relative displacements. Coefficient weighting of the relative displacements can prevent vertical physical limit stoppers from colliding between the car body and bogie when the vertical displacement becomes very large. In this study, in order to achieve the maximum effect of vibration control, a limit was set for the maximum root-mean-squared (RMS) value of the forces generated by each actuator, r was set to a constant value, and q_1 and q_2 were varied to determine a combination of values that result in maximum improvement of ride comfort, within the defined limits of the actuator output. The weighting coefficients used in this study are shown in Table 2. This control method was compared with the case of optimal preview control without frequency shaping, in which the weighting coefficients were derived in a similar manner. Each car body and bogie was assumed to be symmetric in the longitudinal direction, such that the effective masses on which each controller acts consists of the front and rear halves of the bogie mass $m_{bf} = m_{br}$ and car body No. 2 mass $m_{cf} = m_{cr}$. The rear car body mass is evenly distributed, such that $m_{cf} = m_{cr} = m_c / 3$.

Table 2: Weighting coefficients used in frequency-shaped optimal preview control

Coefficient	q_1	q_2	r
Value	10^7	10^{10}	1

4.2 Maximum force control of the primary suspension using the linear generator device

As discussed in Chapter 2, the bogie-integrated linear generator device can generate additional electromagnetic forces that can be applied to the vibration control of the primary suspension. Suzuki [5] mentions that the forces output by this linear generator device are relatively small for the requirements vibration control of the primary suspension. In order to fully utilize the forces generated by the bogie-integrated linear generator device, the maximum possible force output by the linear generator device is used at all times, with the polarity of the force switched according to the polarity of the bogie vertical velocity as expressed in Equation 10 (Suzuki [5]).

$$F_{mz} = -\text{sign}(\dot{z}_b) \cdot f_{mz} \quad (10)$$

Here, F_{mz} represents the control force and f_{mz} the maximum possible vertical force output by the linear generator device. The computations assume that the bogie vertical velocity \dot{z}_b which is the control feedback variable is derived by using accelerometers to measure the acceleration of the vertical vibration of the bogie, then integrating this acceleration once to derive the absolute velocity. Equation 10 was added to the dynamic equations of the vertical motions of all four bogies in Equation 5. The computations assume that the control force of each bogie can be applied independently of each other.

5 MODEL GUIDEWAY IRREGULARITIES FOR EXTERNAL DISTURBANCE INPUT AND RIDE COMFORT LEVELS

To assess the effectiveness of the vibration control method, irregularities in the vertical alignment of ground coils along the sidewalls of the guideway (vertical irregularities) were generated, and used as external disturbance input in time domain simulations. A transfer function was formed based on Watanabe [7], and a uniformly random number was used to compute the vertical irregularities. This transfer function has the characteristic of flattening out at low frequencies in order to reduce the amplitude of vibrations in low frequency ranges. The power spectral density (PSD) of the vertical irregularities is shown in Figure 6.

The ride comfort level, a quantitative index for passenger comfort based on the car body acceleration response to vertical irregularities, was used to

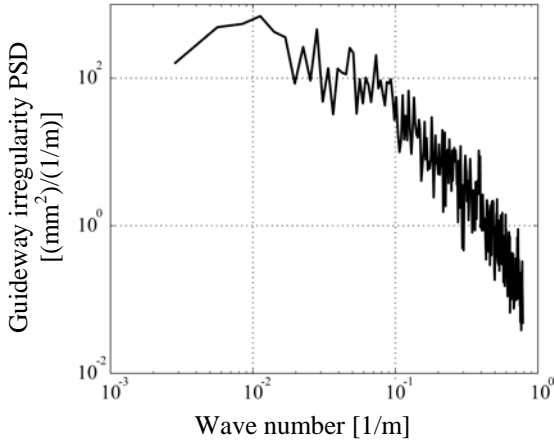


Figure 6. Power spectral density of guideway irregularities.

confirm the performance of the vibration control in this study. This ride comfort level (denoted L_T) is based on ISO 2631 and was devised by the former Japanese National Railways. To derive the L_T value, ride comfort filters based on frequency shaping curves are applied to the vehicle response in the form of the car body vibration acceleration, to account for human perception of vibrations. Next, the resulting value is divided by a reference vibration acceleration value a_{ref} . Finally, the logarithm of the RMS of this value is derived, and expressed in decibels (dB). The following equation was used in this study to compute the ride comfort levels (Tanifuji [6]).

$$L_T = 20 \log_{10}(\alpha_w / a_{ref}) \quad [dB] \quad (11)$$

where

$$\alpha_w^2 = \int_0^\infty W^2(f) \cdot P_{xx} \cdot df \quad (12)$$

$$a_{ref} = 10^{-5} [m/sec^2]$$

Here, $W(f)$ represents the ride comfort filter, and $P_{xx}(f)$ the car body vibration acceleration PSD. Since there are no regulations defining this filter for frequencies below 0.5 Hz, the weighting factor for 0.5 Hz was also used for the frequency range below 0.5 Hz.

6 RESULTS

The following cases were studied as described in this chapter in the sections to follow:

Case 1: Optimal preview control of secondary suspension without frequency shaping.

Case 2: Frequency-shaped optimal preview control of secondary suspension.

Case 3: Maximum force control of primary suspension.

Case 4: Cases 2 and 3 combined.

6.1 Time domain computation results of the secondary suspension control

Time domain simulations were performed with the secondary suspension control, using the vertical irregularities described in the previous chapter. An example of results for a 10-second interval is shown in Figure 7, including the vertical acceleration of the mass center of car body No. 2 and the forces generated by the actuators attached to the two ends of this car body. In this figure, the frequency-shaped optimal preview control case (Case 2) is compared with the uncontrolled passive case and the optimal preview control case without frequency shaping (Case 1). Figure 7b indicates that both of the two controlled cases have acceleration amplitudes smaller than that of the passive case, but it is difficult to see any significant differences between the two controlled cases. In contrast, Figs. 7c and 7d show that the actuator forces have smaller amplitudes in Case 2. In particular, actuator forces in Case 2 are within 1.5 kN, while those of Case 1 reach a maximum of 2.3 kN. Thus, for the same quantity of reduction in the car body acceleration, the frequency-shaped optimal preview control of Case 2 has a higher efficiency, allowing for the design of smaller actuators with smaller maximum forces.

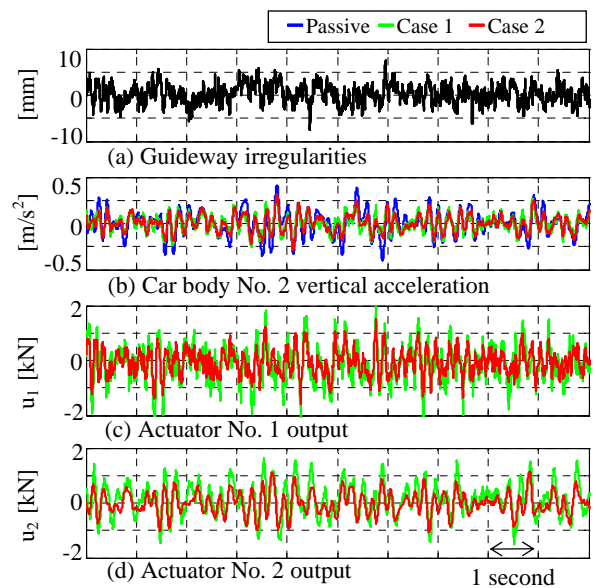


Figure 7. Time domain simulation results for Cases 1 and 2.

6.2 Frequency domain computation results of the secondary suspension control

Next, in the examination of results in the frequency domain, vertical acceleration PSD plots of car body No. 2 were derived from the time domain response described in the previous section, and are shown in Figure 8. The quantity of reduction of the average ride comfort level relative to the reference passive case is displayed in the legend of this figure. The car body PSD peak at around 1 to 2 Hz corresponding to the vertical motions of the car body is larger in Case 2 than in Case 1. However, the frequency shaping factor of the vertical ride comfort level curve is small in this frequency range, such that there is no large difference in effect on the ride comfort level.

At higher frequencies beyond 10 Hz, the frequency shaping factor reduces the effects of the actuator output force, as can be observed by comparing the acceleration output of Cases 1 and 2, resulting in the same order of ride comfort as that of the passive case at these higher frequencies. The ride comfort level in both controlled cases is over 3 dB lower than in the passive case.

6.3 Frequency domain computation results of the primary suspension control

Vertical acceleration PSD plots of car body No. 2 were derived from the time domain response for the maximum force control of the primary suspension, and are shown in Figure 9. The vertical generated force f_{mz} in Equation 10 was set to 2 kN, and applied to each of the four bogies. As defined at the beginning of this chapter, Case 3 represents the maximum force control of the primary suspension

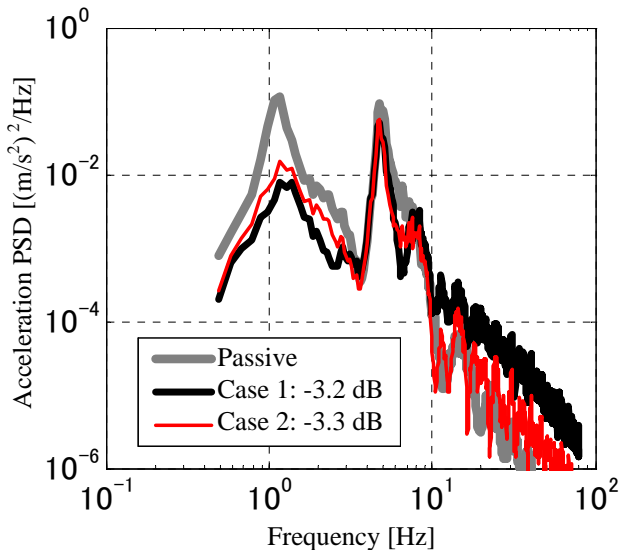


Figure 8. Car body No. 2 center vertical acceleration PSD plots of Cases 1 and 2.

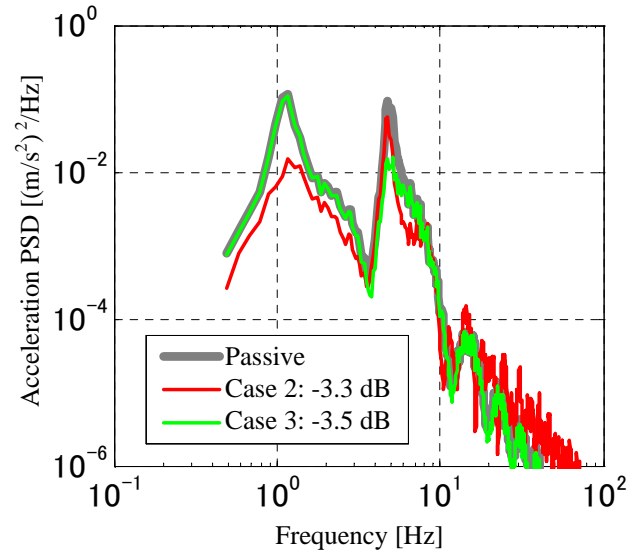
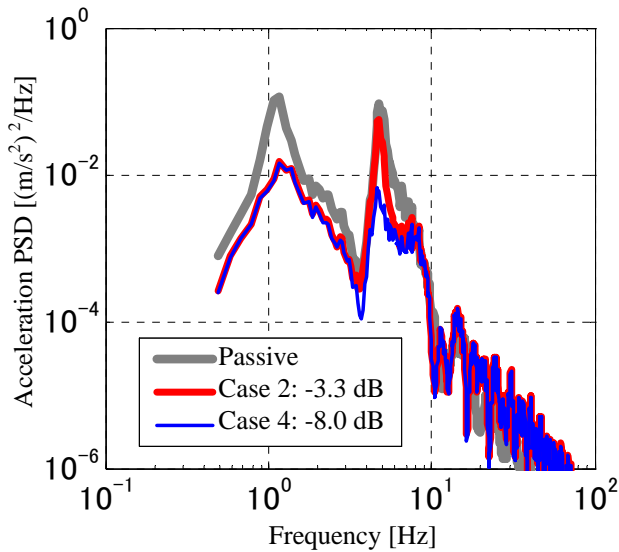


Figure 9. Car body No. 2 center vertical acceleration PSD plots of Cases 2 and 3.

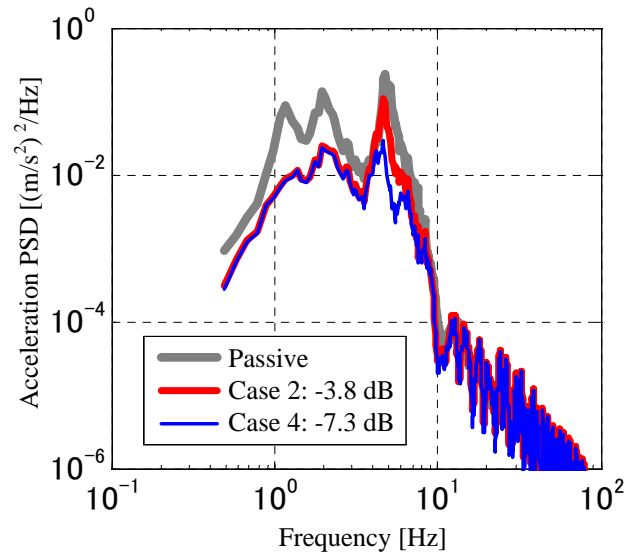
control alone, and Case 2 is the frequency-shaped optimal preview control of the secondary suspension alone. Again, the quantity of reduction of the average ride comfort level relative to the reference passive case is displayed in the legend of this figure. The car body PSD peak at around 1 to 2 Hz corresponding to the vertical motions of the car body has been reduced in Case 2 to about one-seventh of the passive case, while this peak was hardly reduced in Case 3. The peak at around 4 to 5 Hz corresponding to the vertical motions of the bogie is slightly reduced in Case 2, while notably reduced in Case 3, to about one-sixth of the passive case. Although the effect of the control methods are at different frequency ranges, the resulting effect on the ride comfort level is of the same order for both cases, over 3 dB lower than in the passive case.

6.4 Combined primary and secondary suspension control

As defined at the beginning of this chapter, Case 4 combines Case 3, the maximum force control of the primary suspension, with Case 2, the frequency-shaped optimal preview control of the secondary suspension. Vertical acceleration PSD plots of car bodies No. 2 and 3 for Cases 2 and 4 are shown in Figure 10. The PSD peak of car body No. 2 at around 1 to 2 Hz has been reduced in Case 4 to about one-seventh of the passive case, the same as that of Case 2. The peak at around 4 to 5 Hz is slightly reduced in Case 2, while significantly reduced in Case 4, to about one-fifteenth of the passive case. With respect to the passive case, the reduction of ride comfort level in Case 4 is slightly larger than the sums of the



(a) Car body No. 2 center



(b) Car body No. 3 center

Figure 10. Car body center vertical acceleration PSD plots of Cases 2 and 4.

reductions of ride comfort levels in Cases 2 and 3. Similar results are observed in the car body No. 3.

7 CONCLUSIONS

A study was conducted on the effectiveness of applying vibration control to the primary and secondary suspension components in a model of the vertical and pitching motions of the superconducting Maglev vehicle. Results confirmed that a frequency-shaped optimal preview control of the secondary suspension can maintain the same order of ride comfort levels in the middle car body, using 30% less actuator output force than in the case without frequency shaping. The vibration peaks at 1 to 2 Hz and at 4 to 5 Hz were considerably reduced by combining the primary and secondary suspension control methods, and the reduction of the ride comfort level with respect to the passive case is larger than the sums of the reductions of ride comfort levels of each control method applied alone.

This research is financially supported in part by the Ministry of Land, Infrastructure, Transport and Tourism, of the government of Japan.

8 REFERENCES

[1] Hasegawa H., Murai T., and Yamamoto T., "Running Tests of a Combined SC Type Linear Generator," Transactions on

Industry Applications, Institute of Electrical Engineers of Japan, Volume 123-D(2), pages 156-163, 2003.

- [2] Sakamoto Y., Murai T., Kashiwagi T., Tanaka M., Suzuki E., and Yamamoto K., "The Development of Linear Generator System Combined with Magnetic Damping Function," Transactions on Industry Applications, Institute of Electrical Engineers of Japan, Volume 126-D(2), pages 192-198, 2006.
- [3] Shirasaki J., Suzuki E., Watanabe K., Hoshino H., and Nagai M., "Improvement of Vibration Reduction Performance of Superconducting Maglev Vehicles Using Optimal Preview Control," Dynamics and Design Conference (D&D 2007), Japan Society of Mechanical Engineers, Tokyo, Japan, CD-ROM Paper OS11-410, September 25-28, 2007.
- [4] Suzuki E., Shirasaki J., Watanabe K., Hoshino H., and Nagai M., "Comparison of Methods to Reduce Vibrations in Superconducting Maglev Vehicles by Primary Suspension Control," Journal of Mechanical Systems for Transportation and Logistics, Japan Society of Mechanical Engineers, Volume 1, Number 1, pages 3-13, 2008.
- [5] Suzuki E. and Watanabe K., "Results of Vibration Control of a Maglev Vehicle Utilizing a Linear Generator," ASME International Design Engineering Technical Conferences and Computers and Information in Engineering Conference (IDETC/CIE), American Society of Mechanical Engineers, Long Beach, CA, U.S.A., CD-ROM Paper DETC2005-84980, September 24-28, 2005.
- [6] Tanifuji K., Yoshioka H., and Miyashita T., "A Prediction of Riding Comfort with an Artificial Generation of Track Irregularity," Transactions of the Japan Society of Mechanical Engineers, Edition C, Volume 56, Number 523, pages 573-577, 1990.
- [7] Watanabe K., Yoshioka H., Suzuki E., Tohtake T., and Nagai M., "A Study of Vibration Control Systems for Superconducting Maglev Vehicles," Journal of System Design and Dynamics, Japan Society of Mechanical Engineers, Volume 1, Number 4, pages 703-713, 2007.